OCEANOGRAPHY

Rapid shifts in circulation and biogeochemistry of the Southern Ocean during deglacial carbon cycle events

Tao Li[1,2]*, Laura F. Robinson[2], Tianyu Chen[1,2], Xingchen T. Wang[3], Andrea Burke[4], James W. B. Rae[4], Albertine Pegrum-Haram[2,5], Timothy D. J. Knowles[6], Gaojun Li[1], Jun Chen[1], Hong Chin Ng[2], Maria Prokopenko[7], George H. Rowland[2], Ana Samperiz[2], Joseph A. Stewart[2], John Southon[8], Peter T. Spooner[2,9]

The Southern Ocean plays a crucial role in regulating atmospheric CO_2 on centennial to millennial time scales. However, observations of sufficient resolution to explore this have been lacking. Here, we report high-resolution, multiproxy records based on precisely dated deep-sea corals from the Southern Ocean. Paired deep ($\Delta^{14}C$ and $\delta^{11}B$) and surface ($\delta^{15}N$) proxy data point to enhanced upwelling coupled with reduced efficiency of the biological pump at 14.6 and 11.7 thousand years (ka) ago, which would have facilitated rapid carbon release to the atmosphere. Transient periods of unusually well-ventilated waters in the deep Southern Ocean occurred at 16.3 and 12.8 ka ago. Contemporaneous atmospheric carbon records indicate that these Southern Ocean ventilation events are also important in releasing respired carbon from the deep ocean to the atmosphere. Our results thus highlight two distinct modes of Southern Ocean circulation and biogeochemistry associated with centennial-scale atmospheric CO_2 jumps during the last deglaciation.

INTRODUCTION

The Southern Ocean is a region of active upwelling (*1*), where deep, carbon- and nutrient-rich water is brought to the surface ocean, providing surface biota with excess major nutrients (nitrogen and phosphorus). Limitation of primary productivity by iron and light deficiency in surface waters (*2*) leaves a substantial fraction of these nutrients unused (Fig. 1A) before they are transported back to the ocean interior, thus allowing CO_2 to escape to the atmosphere (*3*). It has been suggested that changes in the circulation and biogeochemistry of the Southern Ocean have driven atmospheric CO_2 variations during glacial-interglacial cycles (*3*) and will exert an important influence on uptake of anthropogenic carbon in the future (*4*). However, coupled general circulation models struggle to fully capture changes in the circulation and biogeochemistry of this region (*5*). Hence, with limited data connecting surface and deep processes, it remains difficult to test the linkages between different modes of oceanic overturning and carbon cycle events, particularly on centennial to millennial time scales.

Paleoclimatic records provide key insights into different modes of Southern Ocean circulation and biogeochemistry and have indicated that the Southern Ocean carbon leak was smaller during the ice ages (*6*–*8*), with more carbon stored in deep ocean (*9*), partly accounting for the lower atmospheric CO_2 (*3*). Proposed mechanisms include upper ocean stratification (*10*), increased iron availability (*2*), reduced overturning of deep water linked to changes in the westerly winds (*11*), reorganization of surface buoyancy fluxes (*12*), and expansion of sea ice that directly blocks CO_2 exchange between surface ocean and atmosphere (*13*). The millennial- and centennial-scale atmospheric CO_2 events of the last deglaciation (*14*) provide an excellent opportunity to test the operation and relative importance of these mechanisms, but such tests require well-dated, high-resolution records of both the physical and biological processes in the Southern Ocean that are comparable with the ice core records (*15*). As yet, there exists no coherent multiproxy dataset on a single high-precision age scale, hindering our ability to deconvolve the relative roles of physical and biological processes of the Southern Ocean in deglacial carbon cycle events.

Here, we use deep-sea scleractinian corals to address this gap in our knowledge of the coupled system, with a multiproxy approach that includes tripling the resolution of previous radiocarbon records. A key advantage of deep-sea corals is that they can be absolutely dated using uranium-series disequilibrium methods (*16*) to provide accurate and precise age control on the various paleoclimate proxies hosted within their skeletons. The radiocarbon content of these corals, after correction for postmortem decay based on their uranium-thorium (U-Th) ages, documents the contemporary $^{14}C/^{12}C$ ratios of dissolved inorganic carbon in ambient seawater (*17*). Radiocarbon is produced by cosmic ray–induced nuclear reaction in the upper atmosphere; thus, its subsequent decay (half-life of 5730 years) in the subsurface ocean provides us a tool with which to trace the rate of deep circulation and carbon exchange between ocean interior and atmosphere in the geological past (*8*, *18*–*21*). The boron isotope composition ($\delta^{11}B$, ‰) of deep-sea corals records seawater pH variations, which serves as a sensitive measure of the ocean carbonate system and can be used to track changes in carbon storage in the ocean interior (*9*). The nitrogen isotope composition ($\delta^{15}N$, ‰) of fossil-bound organic matter in deep-sea corals can record the degree of nitrate consumption in the surface ocean, as deep-sea corals feed on sinking organic matter from the surface ocean where phytoplankton preferentially assimilates ^{14}N relative to ^{15}N (*6*, *22*). Together,

[1]MOE Key Laboratory of Surficial Geochemistry, Department of Earth and Planetary Sciences, Nanjing University, Nanjing, China. [2]School of Earth Sciences, University of Bristol, Bristol, UK. [3]Department of Earth and Environmental Sciences, Boston College, Chestnut Hill, MA, USA. [4]School of Earth and Environmental Sciences, University of St Andrews, St Andrews, UK. [5]School of Earth Science and Engineering, Imperial College London, London, UK. [6]Bristol Radiocarbon Accelerator Mass Spectrometry Facility, School of Chemistry and School of Arts, University of Bristol, Bristol, UK. [7]Department of Geology, Pomona College, Claremont, CA, USA. [8]School of Physical Sciences, University of California, Irvine, Irvine, CA, USA. [9]Department of Geography, University College London, London, UK.
*Corresponding author. Email: taoli.es.nju@gmail.com

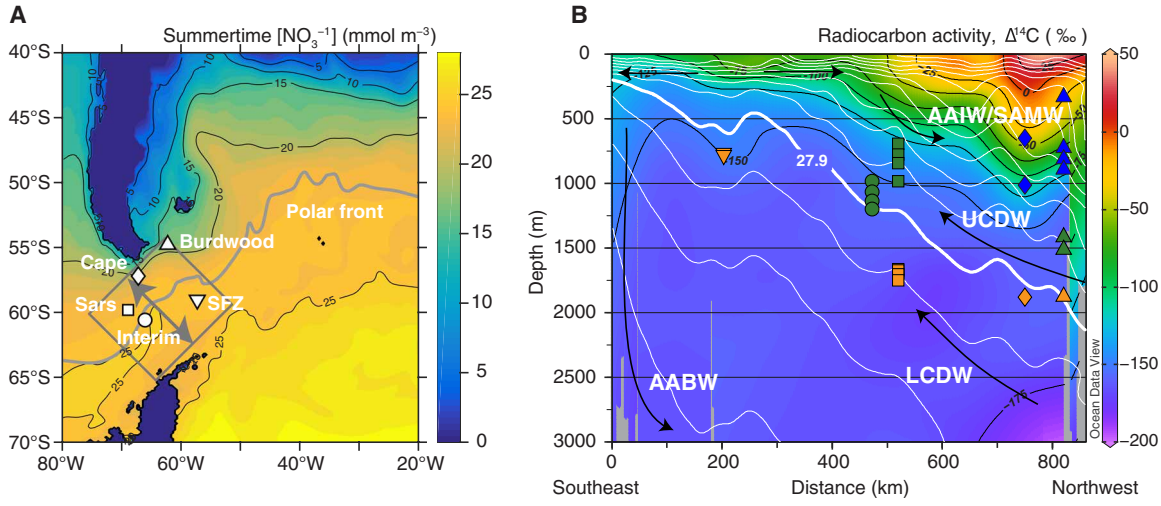

Fig. 1. Locations of Drake Passage deep-sea corals. (**A**) Map showing averaged summertime surface nitrate concentration [B-SOSE (Biogeochemical Southern Ocean State Estimate) data (*62*)] (color scale), current position of the polar front (gray line), and sampling sites (open symbols), including Burdwood Bank (triangle), Cape Horn (diamond), Sars Seamount (square), Interim Seamount (circle), and Shackleton Fracture Zone (SFZ) (downward triangle). (**B**) Vertical profile of bomb-corrected radiocarbon activity ($\Delta^{14}C$) from GLODAP-2 (Global Ocean Data Analysis Project version 2) dataset (*63*) for the area highlighted with gray rectangle in (A). Neutral density contours (white lines) are shown with 27.9 kg m^{-3} line highlighted. Distance is measured along the gray arrow in (A) perpendicular to the polar front from southeast to northwest. Symbols are the same as in (A) and have been separated into deep (orange), intermediate (green), and shallow (blue) layers. LCDW, Lower Circumpolar Deep Water; AABW, Antarctic Bottom Water. (B) has been plotted using Ocean Data View software (*64*).

the combined coralline ^{14}C, $\delta^{11}B$, and $\delta^{15}N$ records have the potential to provide invaluable information on physical and biological processes operated in the Southern Ocean with accurate age control. Direct comparison to high-resolution ice core records of atmospheric CO_2 enables us to better understand the interaction among ocean circulation, biological activity, and the global carbon cycle during the rapid carbon cycle changes of the last deglaciation.

Deep-sea scleractinian coral samples were recovered from seamounts in the Drake Passage (Fig. 1A), from water depths ranging from 1879 to 316 m and bathed today by Upper Circumpolar Deep Water (UCDW), Antarctic Intermediate Water (AAIW), and Subantarctic Mode Water (SAMW) (Fig. 1B). Samples were precisely dated by isotope dilution U-Th dating (*16*), and those with low initial ^{232}Th concentrations (and thus the highest precision calendar ages) were then selected for radiocarbon measurement (fig. S1). A radiocarbon parameter related to the isolation (in terms of circulation and air-sea gas exchange) of the paleowater mass, B-Atmosphere (B-Atm.), was calculated as the radiocarbon age difference between the seawater and the contemporaneous atmosphere (see Materials and Methods). Augmenting this new ^{14}C record, we include previously published $\delta^{15}N$ (*6*) and $\delta^{11}B$ (*9*) records with the same precise U-Th ages based on the calibrated coral species (*Desmophyllum dianthus*). The coral $\delta^{15}N$ data on the new U-Th age scale reveal transient intervals characterized by low degree of surface nutrient utilization during the last deglaciation, which were obscured in previous work that relied on a less precise "reconnaissance" time scale (*6*) with age uncertainties sometimes over 1000 years (fig. S2).

RESULTS

The unprecedented spatial and temporal resolution of our Southern Ocean records enables us to group the ^{14}C data into three different oceanographic layers (Fig. 1 and fig. S3). The shallow layer, bathed today by AAIW and SAMW, generally follows the atmospheric $\Delta^{14}C$ curve (Fig. 2A) (*23*) but with a greater $\Delta^{14}C$ offset ($\Delta\Delta^{14}C$) from the contemporaneous atmosphere during the Last Glacial Maximum [LGM; ~22 to 18 thousand years (ka) ago; −230‰; ~1400 B-Atm. years] than the Holocene (−100‰; ~650 B-Atm. years) (figs. S3 and S4). The deep layer, occupied by UCDW today, shows the most ^{14}C-depleted signal (Fig. 2B), with a radiocarbon offset from the contemporaneous atmosphere of up to −340‰ (~2100 B-Atm. years) during the LGM, compared to just −160‰ (~1200 B-Atm. years) during the Holocene. This deep layer became better ventilated over the course of the last deglaciation, with marked excursions to ^{14}C-enriched values (very low B-Atm. ages of ~300 to 500 years) at 16.3 and 12.8 ka ago (Fig. 3F). The intermediate layer, located in the transition zone between AAIW and UCDW today (Fig. 1B), has $\Delta^{14}C$ values that lie between the deep and shallow layers during the LGM and much of the deglaciation (Fig. 2). This $\Delta^{14}C$ gradient was eroded by the early Holocene, with the intermediate layer displaying similar values to the deep layer (Fig. 2B), similar to the modern water column of the Southern Ocean (Fig. 1B).

DISCUSSION

During the LGM, the combined coral ^{14}C, $\delta^{11}B$, and $\delta^{15}N$ records support the hypothesis of limited exchange between the surface and deep Southern Ocean (*3*, *8*, *10*) (Fig. 3 and fig. S6). The large radiocarbon age offsets from the contemporaneous atmosphere (~2100 to 1400 years) seen at all depths (Fig. 3, E and F) indicate enhanced isolation of the deep Southern Ocean, which is likely linked to some combination of northward shifted frontal systems under cold climate (*11*), surface ocean stratification (*10*), and reduced air-sea gas exchange due to an expansion of sea ice (*13*). This is also corroborated by deep-sea coral ^{14}C data from South of Tasmania (*24*), which show similarly increased radiocarbon age offsets from the contemporaneous

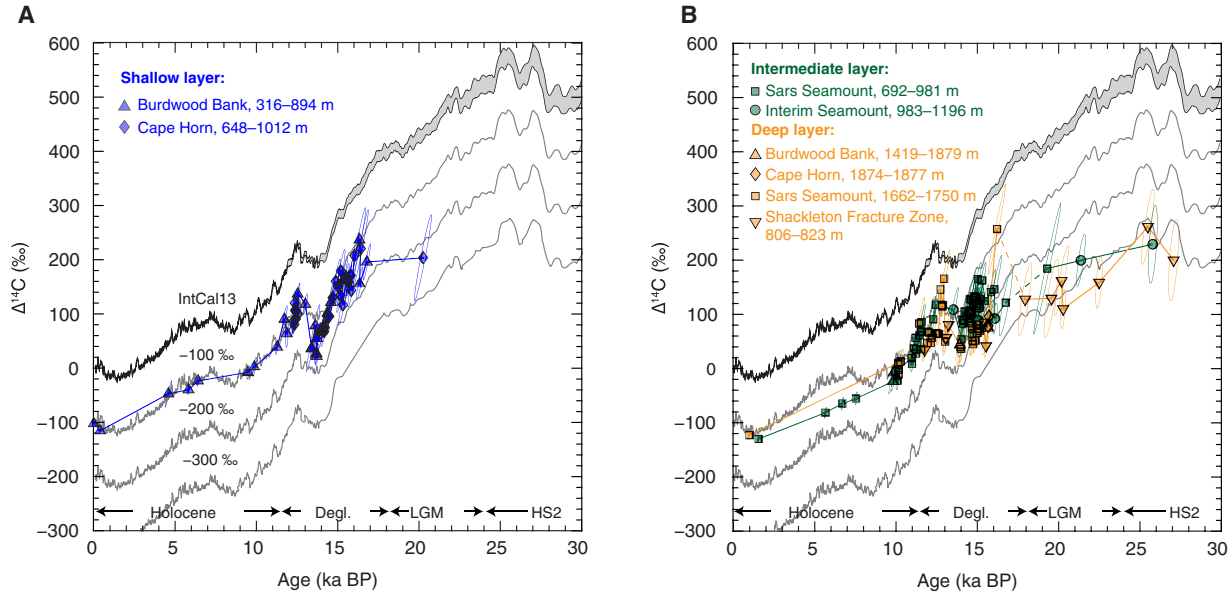

Fig. 2. Radiocarbon variability in the Drake Passage reconstructed from deep-sea corals. (**A**) Reconstructed radiocarbon activity ($\Delta^{14}C$) of deep-sea corals from the shallow layer (blue) (Fig. 1B). Error ellipses denote 2σ uncertainties. The gray area represents the atmospheric $\Delta^{14}C$ curve (*23*) (±2σ uncertainties, gray envelope) and shifts of −100, −200, and −300‰ for better comparison with the coral radiocarbon records. (**B**) Reconstructed $\Delta^{14}C$ of deep-sea corals from the intermediate (green) and deep (orange) layers (Fig. 1B). Symbols are the same as in Fig. 1B. Degl., last deglaciation; HS2, Heinrich Stadial 2. Thousand years before present (ka BP) refers to age before 1950 CE.

atmosphere during the LGM (fig. S5). Increased isolation of waters at depth at the LGM is further supported by a more pronounced ^{14}C gradient between our deep-sea coral–based ^{14}C reconstruction and South Atlantic foraminiferal-based ^{14}C reconstruction of waters currently bathed by the deeper Lower Circumpolar Deep Water (LCDW) (fig. S7) (*7*). Low $\delta^{11}B$ pH values seen in the deep layers (Fig. 3G and fig. S6) point to enhanced dissolved inorganic carbon storage in the deeper glacial Southern Ocean (*9*). At the same time, high $\delta^{15}N$ values indicate an efficient biological pump, with surface nitrate being largely consumed in the Antarctic Zone (AZ) (Fig. 3H and fig. S6) (*6*). Given low export productivity (Fig. 3I) (*25*), this high efficiency is very likely caused by restricted nitrate supply from the deep ocean to the surface (*6*, *26*). These LGM data highlight the value of multiproxy deep-sea coral records in documenting the ocean circulation and biological activity in the Southern Ocean in sequestering carbon from the atmosphere and storing carbon in the deep ocean during the last ice ages (*3*, *10*).

Over the course of the last deglaciation, the radiocarbon age offsets from the contemporaneous atmosphere are progressively diminished, with B-Atm. ages at all depths approaching the late Holocene value (~950 years) (Fig. 2 and fig. S6). This happens alongside breakdown in the pH gradient between the deep and intermediate layers (*9*), rising export productivity, and a decrease in the efficiency of the surface biological pump (Fig. 3 and fig. S6) (*6*). These combined signals in our data point to ventilation of the Southern Ocean interior and upwelling of carbon- and nutrient-rich deep waters, enhancing export productivity but driving the biological pump toward lower overall efficiency. In this scenario, substantial amounts of upwelled carbon would evade removal by surface biomass or transport back to the ocean interior and escape to the atmosphere, likely contributing to atmospheric CO_2 rise at these times.

The initial phase of the deglacial transition [early Heinrich Stadial 1 (HS1), ~18.0 to 16.3 ka ago] was characterized by rising atmospheric CO_2 and marked drops in its $\delta^{13}C$ and $\Delta^{14}C$, along with rising Antarctic temperatures and retreating sea ice (Figs. 2 and 3 and fig. S6). However, there is little resolvable change in coral records of ^{14}C ventilation compared to the contemporaneous atmosphere and no resolvable changes in coral $\delta^{15}N$ records (fig. S6). Release of old carbon from the deep ocean to the atmosphere within the AZ would be expected to cause changes in deep ocean ventilation and the extent of surface nitrate consumption, neither of which are supported by the deep-sea coral data. Our results therefore suggest that processes operating in the AZ likely played a minor role in the initial deglacial CO_2 rise. Other regions and processes may have played a more important role at this time, such as reduced iron fertilization in the Subantarctic Zone of the Southern Ocean, associated with declining dust flux (fig. S8) (*27*, *28*), or increased ventilation of the North Pacific (fig. S7) (*29*–*31*).

Superimposed on the overall deglacial CO_2 rise are a number of abrupt events where atmospheric CO_2 increased by up to ~13 parts per million in 100 years (*14*). These events appear to fall into two categories with distinct climatic and oceanographic characteristics. Rising CO_2 at 14.6 and 11.7 ka ago was associated with rapid warming in the Northern Hemisphere (Fig. 3C) (*32*), resumption of the Atlantic meridional overturning circulation (AMOC) (Fig. 3D) (*18*, *33*), a northward shift of the Southern Hemisphere westerly winds (*34*), and rapid drops in atmospheric $\Delta^{14}C$ (Fig. 4C). In distinct contrast, CO_2 rises at 16.3 and 12.8 ka ago were associated with Northern Hemisphere cooling (Fig. 3C), reduced AMOC, and a shift of the westerlies toward Antarctica (*34*), along with distinctive drops in atmospheric $\delta^{13}C$ and minima in atmospheric $\Delta^{14}C$ (Fig. 4, B and C). The resolution and dating precision of the new coral-based data provide a unique opportunity to connect changes in the circulation and biogeochemistry of the Southern Ocean to these distinctive rises in atmospheric CO_2 (*14*).

During the events associated with rapid Northern Hemisphere warming (14.6 and 11.7 ka ago), we observe pronounced low values

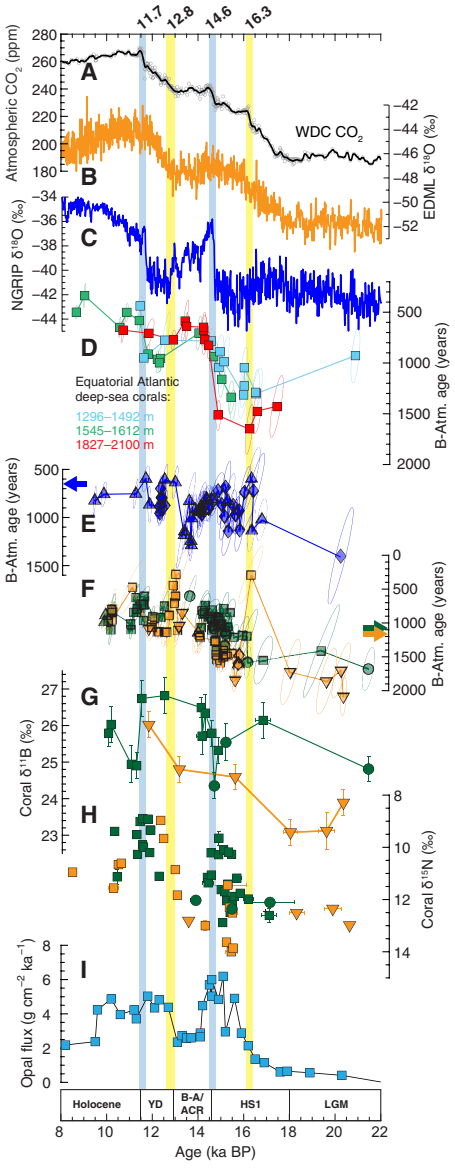

Fig. 3. Comparison of deep-sea coral radiocarbon, boron, and nitrogen isotopic records with other paleoclimatic records of the last deglaciation. (**A**) High-resolution atmospheric CO_2 concentration record from the West Antarctic Ice Sheet Divide ice core (WDC) (circles; gray line is 50 years moving average) (*14*). (**B** and **C**) Ice core $\delta^{18}O$ records (air temperature proxy) smoothed with a 50-year running mean from Antarctic (EDML) (orange) (*65*) and northern Greenland [NGRIP (North Greenland Ice Core Project)] (blue) (*66*) ice cores. The EDML records have been rescaled on the Antarctic Ice Core Chronology 2012 (AICC2012) time scale (*67*). (**D**) Reconstructed Equatorial Atlantic deep-sea coral B-Atm. ages for different water depth ranges: 1296 to 1492 m (blue), 1545 to 1612 m (green), and 1827 to 2100 m (red) (*18*). Error ellipses denote 2σ uncertainties. (**E** and **F**) Deep-sea coral B-Atm. ages for the shallow (blue), intermediate (green), and deep (orange) layers. Error ellipses denote 2σ uncertainties. Arrows represent the modern radiocarbon age difference between different layers and the atmosphere. Colors and symbols are the same as in Fig. 2. (**G**) Deep-sea coral boron isotopes for the intermediate (green) and deep (orange) layers (*9*). Colors and symbols are the same as in Fig. 2. (**H**) Deep-sea coral nitrogen isotopes for the intermediate (green) and deep (orange) layers in the Antarctic Zone (AZ) of the Southern Ocean (*6*). (**I**) Opal flux in the Atlantic Ocean sector of AZ (core TN057-13-4PC) (*25*). Light blue bands denote the centennial events at 14.6 and 11.7 ka ago, while yellow bands highlight the centennial events at 16.3 and 12.8 ka ago. ppm, parts per million; B-A/ACR, Bølling-Allerød/Antarctic Cold Reversal; YD, Younger Dryas.

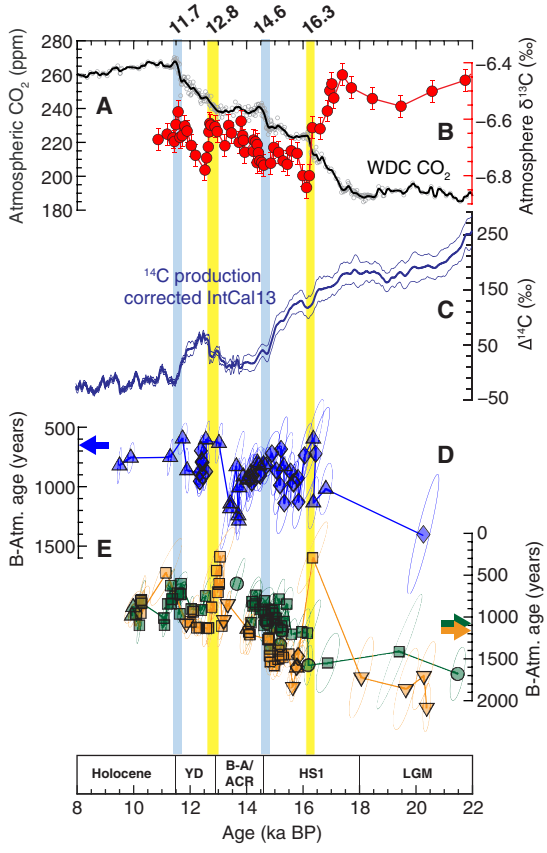

Fig. 4. Comparison of deep-sea coral radiocarbon records with atmospheric carbon records of the last deglaciation. (**A**) High-resolution atmospheric CO_2 concentration record from the WDC (circles; gray line is 50 years moving average) (*14*). (**B**) Atmospheric $\delta^{13}C$ record from Taylor Glacier, Antarctica (*42*). (**C**) ^{14}C production corrected atmospheric $\Delta^{14}C$ curve. Variations of atmospheric $\Delta^{14}C$ caused by changing cosmogenic ^{14}C production rate, which is controlled by the strength of Earth's magnetic field, were subtracted from the IntCal13 compilation (*23*, *68*, *69*). (**D** and **E**) Deep-sea coral B-Atm. ages for the shallow (blue), intermediate (green), and deep (orange) layers. Error ellipses denote 2σ uncertainties. Arrows represent the modern radiocarbon age difference between different layers and the atmosphere. Colors and symbols are the same as in Fig. 2. Light blue bands denote the centennial events at 14.6 and 11.7 ka ago, while yellow bands highlight the centennial events at 16.3 and 12.8 ka ago.

in coral $\delta^{15}N$ records, very low pH at intermediate depth, and relatively well-ventilated ^{14}C conditions at all depths (Fig. 3). When considered in conjunction with the high opal flux in the AZ (Fig. 3I) (*25*), these combined signals point to strong upwelling of carbon- and nutrient-rich deep waters, giving rise to enhanced export productivity but a less efficient surface biological pump. This scenario would allow rapid release of respired carbon from the deep ocean to the upper ocean and the atmosphere (Fig. 3A) and, alongside strengthened AMOC, may contribute to decreases in atmospheric $\Delta^{14}C$ (Fig. 4C). The coral ^{14}C data do not show such extreme changes as seen in pH and $\delta^{15}N$ records (fig. S9), likely reflecting a balance between mixing up of old ^{14}C-depeleted deep waters and enhanced air-sea gas exchange and ventilation associated with shifts in the westerly winds (*34*). In detail, the coral ^{14}C data appear to show a slight younging at depth but little change in the upper ocean (fig. S9), consistent with increased ventilation being compensated by the

transfer of old carbon from deeper to shallower layers. We also note that although the coral $\delta^{15}N$ records show changes in the preceding millennia and exhibit some short time scale variability (*6*), there is a shift in the mean state of these data to reach minimum values centered on these events (Fig. 3H). These transient events were coincident with the rapid resumption of the AMOC, including an overshoot in the formation of North Atlantic Deep Water (NADW) Fig. 3D) (*18*, *33*), as well as rapid Northern Hemisphere warming (Fig. 3C), which is thought likely to have triggered changes in the Southern Ocean (*9*, *18*, *34*, *35*). For instance, an associated northward shift in the westerlies (*34*) and the Southern Ocean fronts may have expanded the region of upwelling of carbon-rich water (*36*, *37*), although the locus of the most intense upwelling is likely to move north. Once oceanic cooling is established, via the bipolar seesaw (*38*), expansion of sea ice would reduce wind-driven mixing and CO_2 outgassing (*9*), accounting for the transient nature of these signals (Fig. 5A).

The oceanic characteristics of two as yet enigmatic times of rising CO_2 at 16.3 and 12.8 ka ago are in marked contrast to the events that are linked to rapid Northern Hemisphere warming (Fig. 3C and fig. S9). The 16.3-ka-ago event is a clear centennial CO_2 jump, while the 12.8-ka-ago event is the start of a more gradual, multicentennial CO_2 rise. Both time periods are associated with distinctive negative excursions of atmospheric $\delta^{13}C$ and $\Delta^{14}C$ (Fig. 4, B and C), AMOC weakening (*33*, *39*), Northern Hemisphere cooling, and Antarctic warming (Fig. 3). Our new deep-sea coral data reveal marked increases in ^{14}C ventilation of a nature not hitherto seen in the Southern Ocean, which are particularly apparent in the deep and shallow layers (Fig. 4). For instance, corals at 1700 m show a shift in radiocarbon age of around 1000 years to reach B-Atm. age offsets of only 300 to 500 years, much better ventilated than modern water masses at these sites (which have B-Atm. ages of ~1200 years) and similar to low-latitude surface waters that have reached full ^{14}C equilibrium with the atmosphere. Given the inefficient nature of ^{14}C ventilation in this region today (*40*), dominated by upwelling of old waters and limited atmospheric ^{14}C exchange, these transient events represent a major departure from the modern Southern Ocean circulation regime.

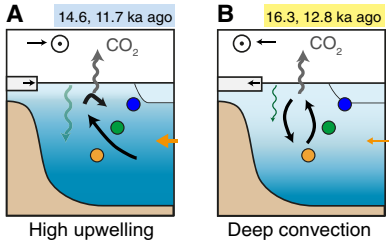

Fig. 5. Schematic of proposed centennial-scale changes in circulation and biogeochemical cycling and productivity in the Southern Ocean. (**A**) During the 14.6- and 11.7-ka-ago events associated with stronger formation of NADW (orange arrow), pronounced upwelling (black arrow) of old, carbon-rich, and nutrient-rich water (dark blue shading) to the upper reaches of the Southern Ocean is indicated by low-pH values seen in the upper ocean corals (Fig. 3G). This high carbon and nutrient flux drove elevated export productivity but with low efficiency of nutrient utilization (long green wavy arrow but with transparent shading), leading to rapid release of respired carbon from the deep ocean to the upper ocean and the atmosphere (gray wavy arrow). These events were also associated with a rapid northward jump in the westerly winds (circle with dot) and a slower expansion of sea ice (rectangle) (*9*). (**B**) During the 16.3- and 12.8-ka ago events associated with weaker formation of NADW, exceptionally ^{14}C-rich water (light blue shading) is found at all coral cites. Export productivity was relatively low, while the nutrient utilization became efficient (short dark green wavy arrow), as carbon- and nutrient-rich waters were flushed out (black arrows) and replaced with well-ventilated surface waters. These events were also associated with a rapid southward shift in the westerly and more slowly retreating sea ice.

These ventilation events were short-lived, persisting for less than 400 years, and were followed by a rapid return to older ^{14}C values close to the pre-excursion conditions. Although these time intervals were also associated with a southward shift in the Southern Hemisphere westerlies (*34*), it seems unlikely that associated changes in water mass distribution (i.e., greater contribution of well-ventilated waters from further north) can explain these radiocarbon excursions seen in the deep layer, given that frontal positions were likely still further north than during the Holocene (*41*). Furthermore, given the persistence of cold conditions in the north and continued warming in the south following these events (*42*), there is no reason to expect (nor evidence for) a northward frontal shift only a few hundred years after the onset of these events to explain the return to older ^{14}C values. Instead, we invoke transient deepening of the mixed layer, perhaps associated with the onset of open-ocean convection, to explain the young radiocarbon ages at these times (Fig. 5B). Deepening of the mixed layer, alongside increased air-sea gas exchange and reduced reservoir ages, has the potential to more efficiently bring ^{14}C-enriched surface waters to depth compared to mixing along isopycnals (*40*). Open convection has been observed in the modern Southern Ocean (*43*), and it is a relatively common feature of coupled climate models, where it occurs associated with shifts in the westerly winds and the sea ice edge (*44*) or changes in stratification associated with NADW weakening (*45*), consistent with conditions during these events. Whatever the exact mechanism, this pronounced ventilation of carbon in the Southern Ocean's interior is likely to have allowed outgassing of old, respired carbon from deep waters to the upper ocean and the atmosphere, driving the rapid rises in atmospheric CO_2 and distinctive drops in atmospheric $\Delta^{14}C$ and $\delta^{13}C$ at these times (Fig. 4).

Although a decrease in atmospheric $\delta^{13}C$ would also be expected from Southern Ocean CO_2 release during the 14.6- and 11.7-ka-ago events, it has been suggested that this potential reduction was overwhelmed by the impact of extensive surface ocean warming in the Northern Hemisphere (Fig. 3) (*42*). The scarcity of well-calibrated coral species during the 16.3- and 12.8-ka-ago events limits the current data resolution of both $\delta^{11}B$ and $\delta^{15}N$ records. However, the available $\delta^{15}N$ data within AZ hint at a muted response in biological pump efficiency, which may reflect the competing influences of enhanced vertical mixing but with increasingly well-ventilated and nutrient-depleted waters. At the end of these events, the mixed layer shoaled and deep convection stopped, a likely consequence of persistent bipolar seesaw-driven warming of the Southern Ocean surface (*34*, *38*), allowing ^{14}C-depleted waters to once again occupy these sites. These coral-based data thus provide the first evidence that centennial-scale ventilation events occurred in the Southern Ocean during the rapid CO_2 rise events at 16.3 and 12.8 ka ago.

After these two events, continued southward shift of the westerlies and sea ice edge in response to Southern Hemisphere warming would have enhanced upwelling and mixing in the Southern Ocean and thus promoted persistent transfer of carbon from the ocean interior to the atmosphere on millennial time scales (*25*, *46*). In support of this, a somewhat enhanced ^{14}C gradient is found between the deep and intermediate layers in late HS1 compared to the more

homogeneous ^{14}C distribution during the LGM and early HS1 (Fig. 3F), which may indicate greater mixing of well-ventilated waters from further north into the intermediate layer in response to the shifting winds. Intensified upwelling of carbon- and nutrient-rich deep water into the upper ocean is also suggested by increasing export productivity and decreasing $\delta^{15}N$ and intermediate layer $\delta^{11}B$ signals at the same time (Fig. 3, G to I). This decrease in the extent of surface nitrate utilization and biological pump efficiency and the transfer of low-pH carbon-rich waters into the upper ocean would have allowed substantial release of carbon to the atmosphere during late HS1 and the Younger Dryas. These millennial changes culminated in the centennial-scale events at 14.6 and 11.7 ka ago, interpreted as maxima in upwelling, associated with transient decoupling of the westerlies from ocean temperatures and the sea ice edge (*9*). Carbonate compensation, due to the disturbance in deep ocean pH and carbonate ion concentration, would also facilitate further carbon release on millennial time scales (*47*, *48*). Consistent signals of reorganization in Southern Ocean circulation and biogeochemistry are also seen across a variety of other tracers and sites at these times (*7*, *49*).

In summary, we have tripled the available resolution of well-dated radiocarbon data from the Southern Ocean, and by grouping these data into different oceanographic layers and coupling with pH and biological pump efficiency proxies on a single high-precision age scale, we are able to discern distinctive characteristics of different mechanisms behind millennial- and centennial-scale CO_2 rise during the last deglaciation. These combined data provide compelling evidence for the interconnection between shifts in the circulation and biogeochemistry of the Southern Ocean and atmospheric CO_2. Notably, our results highlight previously undocumented pulses of vigorous ventilation of the deep Southern Ocean, associated with pronounced deepening of the mixed layer, which can facilitate rapid carbon release in the Southern Ocean and explain the mysterious atmospheric CO_2 increases at 16.3 and 12.8 ka ago.

MATERIALS AND METHODS

Drake Passage deep-sea coral sampling

Drake Passage coral samples were recovered from Shackleton Fracture Zone (60°11′S 57°50′W), Interim Seamount (60°36′S 66°0′W), Sars Seamount (59°48′S 68°58′W), Cape Horn (57°10′S 66°06′W), and Burdwood Bank (54°30′S 62°10′W) (Fig. 1A), with water depth ranging from 316 to 1879 m and bathed today mainly by UCDW, AAIW, and SAMW (Fig. 1B). The coral samples were collected using dredges and trawls on three cruises: LMG0605, NBP08-05, and NBP1103 (*8*, *18*). Today, Shackleton Fracture Zone and Interim Seamount are located in the AZ and Sars Seamount is on the polar front, whereas Cape Horn and Burdwood Bank are located in the Subantarctic Zone (Fig. 1A). The deep-sea corals collected at Sars Seamount cover a wide-depth range, with relatively high temporal resolution at 981 and 1701 m for the last deglaciation (fig. S1). Samples from Shackleton Fracture Zone and Interim Seamount only have a limited depth range and are not so highly resolved. Further north, corals collected from Burdwood Bank and Cape Horn are the shallowest samples (316 m) that we investigated here (Fig. 1B and fig. S1).

Coral samples are grouped into three "depth" ranges (deep, intermediate, and shallow) based on the modern geometry of water masses in the Southern Ocean (Fig. 1B) and the reconstructed ^{14}C patterns. The deep layer, bathed today by UCDW, consists of Shackleton Fracture Zone (806 to 823 m), Sars Seamount (1323 to 1750 m), Cape Horn (1874 m), and Burdwood Bank (1419 to 1879 m). The intermediate layer [Sars Seamount (692 to 981 m) and Interim Seamount (1064 to 1196 m)] is also bathed today by UCDW. The shallow layer [Burdwood Bank (318 to 894 m) and Cape Horn (648 to 1012 m)] is located well above the water masses bathed today by UCDW and is occupied by AAIW/SAMW today.

Reconnaissance dating and sample selection

More than 2000 deep-sea corals (*Desmophyllum*, *Caryophyllia*, *Flabellum*, *Balanophyllia*, and *Paraconotrochus*) have been reconnaissance dated with two different methods: laser ablation U-Th dating (*50*) and ^{14}C dating (*51*). Only a quarter of these reconnaissance ages have been reported in prior publications (*18*, *50*–*52*). We do not report all of the reconnaissance ages here but use these new dates for sample selection. The new dating targeted Sars Seamount and Cape Horn using the laser ablation U-Th dating method (*50*) to identify samples needed to complete the study. Previously, 59 deep-sea coral samples from Drake Passage were selected for precise isotope dilution dating and radiocarbon analysis (*8*, *18*). To increase the spatial and temporal resolution of the deep-sea coral radiocarbon records, we selected a further 112 samples, mainly from Sars Seamount (981 and 1701 m), Burdwood Bank (334 m), and Cape Horn (1012 m) (fig. S1). Deglacial deep-sea coral (*D. dianthus*) $\delta^{15}N$ records at the Drake Passage were previously reported on the basis of the less precise reconnaissance time scale (*6*). Here, we have precisely dated 33 more samples with published $\delta^{15}N$ data (fig. S2), together with 20 samples with published paired U-Th ages and $\delta^{15}N$ data, allowing for direct comparison between deep-sea coral ^{14}C and $\delta^{15}N$ records and other climatic records on submillennial time scales.

Isotope dilution U-Th dating

U-series dating was carried out following the established protocols in the Bristol Isotope Group at the University of Bristol (*18*). Briefly, ferromanganese and organic coatings or remineralized parts of the coral samples were carefully removed with a Dremel tool before ~0.2-g samples were cut for chemical cleaning (*16*). Cleaned samples were weighed and dissolved in Teflon beakers using 2 ml of 7 M distilled HNO_3. A ^{236}U-^{229}Th mixed spike was added to each sample and dried down at 180°C on the hot plate. Iron coprecipitation and anion exchange columns were used to purify and separate the U and Th fractions from the matrix. Typically, 10 samples were processed together with one U standard (Harwell uraninite standard, HU1) and one blank (4 ml of 7 M distilled HNO_3) for every batch. U and Th isotope ratios were measured using the standard-sample-bracketing method using a multicollector inductively coupled plasma mass spectrometer (Neptune) connected with an Aridus desolvation system (Cetac). The U112a standard was used to bracket samples during U isotope measurements, whereas an in-house standard (SGS) was used for Th isotope measurements. Quality control was conducted by measuring HU1 and Th standards (ThB) at the beginning of every batch and after every four samples during analysis. We obtained a long-term external precision of ~1‰ for $^{234}U/^{238}U$ ratios and 2‰ for $^{229}Th/^{230}Th$ ratios based on the replicate measurements of both standards. A single uranium spike (^{236}U) was added to the Th fraction and measured on a Faraday cup to normalize the signals during peak jumping between ^{229}Th and ^{230}Th (*8*). The long-term external

reproducibility of [^{230}Th/^{238}U] (activity ratio), which was monitored by repeated measurements of HU1 standard processed through column chemistry, was better than 3‰ (n = 36, 2 SD). For the coral samples, the initial ^{230}Th was corrected on the basis of the modern-day ^{230}Th/^{232}Th ratios of the seawater collected near the dredge sites (*53*) and the measured ^{232}Th concentration. The ages were resolved using the U-series age equations (*54*), and the errors, including those associated with mass bias corrections, procedural blanks, and initial ^{230}Th corrections, were propagated using a Monte Carlo method (*18*).

Relatively large uncertainty in the modern-day ^{230}Th/^{232}Th atomic ratio ($2 \pm 2 \times 10^{-4}$, 2 SD) applied to correct the initial ^{230}Th and in error propagation means that the final age uncertainties strongly depend on the ^{232}Th concentrations (fig. S10B). To minimize the influence of initial ^{230}Th contamination on the final age uncertainties, coral samples with high ^{232}Th concentrations were duplicated to get the lowest possible ^{232}Th concentration. All samples used for radiocarbon analysis have ^{232}Th concentrations less than 2000 pg/g (fig. S10A). Initial δ^{234}U ratios vary from 143.8 to 153.8‰ (fig. S10C), consistent with the δ^{234}U range of a closed-system model, in which we consider the influence of both ocean mixing and glacial river flux on the local seawater ^{234}U budget (*55*) and assume that the initial seawater δ^{234}U ratio is within ±7‰ of the LGM value (144.7‰), deglaciation value (148.7‰), and Holocene value (146.7‰) (fig. S10D) (*54*, *56*, *57*).

Radiocarbon analysis and data processing

The radiocarbon data in this study were measured at the UC Irvine Keck–Carbon Cycle Accelerator Mass Spectrometer facility and Bristol Radiocarbon Accelerator Mass Spectrometry Facility. Sample preparation for radiocarbon analysis followed previously established protocols for the deep-sea corals (*8*, *17*–*19*, *51*). Briefly, about 20 mg of each sample was first leached with 0.1 M L^{-1} HCl to remove potentially adsorbed CO_2 (*17*). Residual samples (~12 mg) were then dissolved in concentrated phosphoric acid in a prevacuumed 5-ml tube. The generated CO_2 gas was graphitized following the hydrogen reduction method (*17*, *58*). The ^{12}C, ^{13}C, and ^{14}C isotopes were measured by accelerator mass spectrometry simultaneously, and the ^{14}C results were normalized to a δ^{13}C value of −25‰ and were reported as fraction modern (Fm) (where modern is defined as 95% of the 1950 CE ^{14}C concentration of the NBS oxalic acid I standard (NIST-SRM-4990) normalized to a δ^{13}C value of −19‰ (*59*)). The blank correction was done by subtracting the Fm of a ^{14}C-dead deep-sea coral from Sars Seamount [~145 ka ago, Fm = 0.0023 ± 0.0011 (n = 23, 2 SD)] from the measured samples.

Radiocarbon activity (Δ^{14}C, ‰) in deep-sea corals was calculated as $\Delta^{14}C_{coral} = (Fm \times e^{(\text{calendar age}/8267)} - 1) \times 1000$ (*60*), where calendar age was obtained by subtracting the time between the year of measurement and the year 1950 from U-Th radiometric age. The Δ^{14}C offset (i.e., $\Delta\Delta^{14}$C) between the seawater and contemporaneous atmosphere was directly calculated as $\Delta^{14}C_{coral} - \Delta^{14}C_{atmosphere}$ (fig. S3). Because $\Delta\Delta^{14}$C is also affected by the changing atmospheric ^{14}C inventory (*8*, *61*), we also calculated B-Atm. age, which is the radiocarbon age difference between the seawater (coral) (*17*) and the contemporaneous atmosphere accounting for the varying atmospheric ^{14}C inventory (*18*). To propagate all of the uncertainties, a Monte Carlo method (*18*) was applied to integrate the errors from ^{14}C measurements, U-Th age determination, and the IntCal13 atmospheric radiocarbon calibration curve (*23*). This method was applied to calculate the error ellipses of Δ^{14}C, $\Delta\Delta^{14}$C, and B-Atm. ages for each sample.

SUPPLEMENTARY MATERIALS

Supplementary material for this article is available at http://advances.sciencemag.org/cgi/content/full/6/42/eabb3807/DC1

REFERENCES AND NOTES

1. J. Marshall, K. Speer, Closure of the meridional overturning circulation through Southern Ocean upwelling. *Nat. Geosci.* **5**, 171–180 (2012).
2. J. H. Martin, Glacial-interglacial CO_2 change: The iron hypothesis. *Paleoceanography* **5**, 1–13 (1990).
3. D. M. Sigman, M. P. Hain, G. H. Haug, The polar ocean and glacial cycles in atmospheric CO_2 concentration. *Nature* **466**, 47–55 (2010).
4. N. Gruber, D. Clement, B. R. Carter, R. A. Feely, S. van Heuven, M. Hoppema, M. Ishii, R. M. Key, A. Kozyr, S. K. Lauvset, C. Lo Monaco, J. T. Mathis, A. Murata, A. Olsen, F. F. Perez, C. L. Sabine, T. Tanhua, R. Wanninkhof, The oceanic sink for anthropogenic CO_2 from 1994 to 2007. *Science* **363**, 1193–1199 (2019).
5. Y. Kostov, J. Marshall, U. Hausmann, K. C. Armour, D. Ferreira, M. M. Holland, Fast and slow responses of Southern Ocean sea surface temperature to SAM in coupled climate models. *Clim. Dynam.* **48**, 1595–1609 (2017).
6. X. T. Wang, D. M. Sigman, M. G. Prokopenko, J. F. Adkins, L. F. Robinson, S. K. Hines, J. Chai, A. S. Studer, A. Martínez-García, T. Chen, G. H. Haug, Deep-sea coral evidence for lower Southern Ocean surface nitrate concentrations during the last ice age. *Proc. Natl. Acad. Sci. U.S.A.* **114**, 3352–3357 (2017).
7. L. C. Skinner, S. Fallon, C. Waelbroeck, E. Michel, S. Barker, Ventilation of the deep Southern Ocean and deglacial CO_2 rise. *Science* **328**, 1147–1151 (2010).
8. A. Burke, L. F. Robinson, The Southern Ocean's role in carbon exchange during the last deglaciation. *Science* **335**, 557–561 (2012).
9. J. W. B. Rae, A. Burke, L. F. Robinson, J. F. Adkins, T. Chen, C. Cole, R. Greenop, T. Li, E. F. M. Littley, D. C. Nita, J. A. Stewart, B. J. Taylor, CO_2 storage and release in the deep Southern Ocean on millennial to centennial timescales. *Nature* **562**, 569–573 (2018).
10. R. Francois, M. A. Altabet, E.-F. Yu, D. M. Sigma, M. P. Bacon, M. Frank, G. Bohrmann, G. Bareille, L. D. Labeyrie, Contribution of Southern Ocean surface-water stratification to low atmospheric CO_2 concentrations during the last glacial period. *Nature* **389**, 929–935 (1997).
11. J. R. Toggweiler, J. L. Russell, S. R. Carson, Midlatitude westerlies, atmospheric CO_2, and climate change during the ice ages. *Paleoceanography* **21**, PA2005 (2006).
12. A. J. Watson, G. K. Vallis, M. Nikurashin, Southern Ocean buoyancy forcing of ocean ventilation and glacial atmospheric CO_2. *Nat. Geosci.* **8**, 861–864 (2015).
13. B. B. Stephens, R. F. Keeling, The influence of Antarctic sea ice on glacial-interglacial CO_2 variations. *Nature* **404**, 171–174 (2000).
14. S. A. Marcott, T. K. Bauska, C. Buizert, E. J. Steig, J. L. Rosen, K. M. Cuffey, T. J. Fudge, J. P. Severinghaus, J. Ahn, M. L. Kalk, J. R. McConnell, T. Sowers, K. C. Taylor, J. W. C. White, E. J. Brook, Centennial-scale changes in the global carbon cycle during the last deglaciation. *Nature* **514**, 616–619 (2014).
15. E. J. Brook, C. Buizert, Antarctic and global climate history viewed from ice cores. *Nature* **558**, 200–208 (2018).
16. H. Cheng, J. Adkins, R. L. Edwards, E. A. Boyle, U-Th dating of deep-sea corals. *Geochim. Cosmochim. Acta* **64**, 2401–2416 (2000).
17. J. F. Adkins, S. Griffin, M. Kashgarian, H. Cheng, E. R. M. Druffel, E. A. Boyle, R. Lawrence Edwards, C. C. Shen, Radiocarbon dating of deep-sea corals. *Radiocarbon* **44**, 567–580 (2002).
18. T. Chen, L. F. Robinson, A. Burke, J. Southon, P. Spooner, P. J. Morris, H. C. Ng, Synchronous centennial abrupt events in the ocean and atmosphere during the last deglaciation. *Science* **349**, 1537–1541 (2015).
19. L. F. Robinson, J. F. Adkins, L. D. Keigwin, J. Southon, D. P. Fernandez, S.-L. Wang, D. S. Scheirer, Radiocarbon variability in the western North Atlantic during the last deglaciation. *Science* **310**, 1469–1473 (2005).
20. E. D. Galbraith, E. Y. Kwon, D. Bianchi, M. P. Hain, J. L. Sarmiento, The impact of atmospheric pCO_2 on carbon isotope ratios of the atmosphere and ocean. *Global Biogeochem. Cycles* **29**, 307–324 (2015).
21. S. J. Goldstein, D. W. Lea, S. Chakraborty, M. Kashgarian, M. T. Murrell, Uranium-series and radiocarbon geochronology of deep-sea corals: Implications for Southern Ocean ventilation rates and the oceanic carbon cycle. *Earth Planet. Sci. Lett.* **193**, 167–182 (2001).
22. X. T. Wang, M. G. Prokopenko, D. M. Sigman, J. F. Adkins, L. F. Robinson, H. Ren, S. Oleynik, B. Williams, G. H. Haug, Isotopic composition of carbonate-bound organic nitrogen in deep-sea scleractinian corals: A new window into past biogeochemical change. *Earth Planet. Sci. Lett.* **400**, 243–250 (2014).

23. P. J. Reimer, E. Bard, A. Bayliss, J. W. Beck, P. G. Blackwell, C. B. Ramsey, C. E. Buck, H. Cheng, R. L. Edwards, M. Friedrich, P. M. Grootes, T. P. Guilderson, H. Haflidason, I. Hajdas, C. Hatté, T. J. Heaton, D. L. Hoffmann, A. G. Hogg, K. A. Hughen, K. F. Kaiser, B. Kromer, S. W. Manning, M. Niu, R. W. Reimer, D. A. Richards, E. M. Scott, J. R. Southon, R. A. Staff, C. S. M. Turney, J. van der Plicht, IntCal13 and Marine13 radiocarbon age calibration curves 0–50,000 years cal BP. *Radiocarbon* **55**, 1869–1887 (2013).
24. S. K. V. Hines, J. R. Southon, J. F. Adkins, A high-resolution record of Southern Ocean intermediate water radiocarbon over the past 30,000 years. *Earth Planet. Sci. Lett.* **432**, 46–58 (2015).
25. R. F. Anderson, S. Ali, L. I. Bradtmiller, S. H. H. Nielsen, M. Q. Fleisher, B. E. Anderson, L. H. Burckle, Wind-driven upwelling in the Southern Ocean and the deglacial rise in atmospheric CO_2. *Science* **323**, 1443–1448 (2009).
26. A. S. Studer, D. M. Sigman, A. Martínez-García, V. Benz, G. Winckler, G. Kuhn, O. Esper, F. Lamy, S. L. Jaccard, L. Wacker, S. Oleynik, R. Gersonde, G. H. Haug, Antarctic Zone nutrient conditions during the last two glacial cycles. *Paleoceanography* **30**, 845–862 (2015).
27. A. Martínez-García, D. M. Sigman, H. Ren, R. F. Anderson, M. Straub, D. A. Hodell, S. L. Jaccard, T. I. Eglinton, G. H. Haug, Iron fertilization of the Subantarctic ocean during the last ice age. *Science* **343**, 1347–1350 (2014).
28. S. L. Jaccard, E. D. Galbraith, A. Martínez-García, R. F. Anderson, Covariation of deep Southern Ocean oxygenation and atmospheric CO_2 through the last ice age. *Nature* **530**, 207–210 (2016).
29. J. W. B. Rae, M. Sarnthein, G. L. Foster, A. Ridgwell, P. M. Grootes, T. Elliott, Deep water formation in the North Pacific and deglacial CO_2 rise. *Paleoceanography* **29**, 645–667 (2014).
30. Y. Okazaki, A. Timmermann, L. Menviel, N. Harada, A. Abe-Ouchi, M. O. Chikamoto, A. Mouchet, H. Asahi, Deepwater formation in the North Pacific during the Last Glacial Termination. *Science* **329**, 200–204 (2010).
31. L. Max, L. Lembke-Jene, J.-R. Riethdorf, R. Tiedemann, D. Nürnberg, H. Kühn, A. Mackensen, Pulses of enhanced North Pacific Intermediate Water ventilation from the Okhotsk Sea and Bering Sea during the last deglaciation. *Clim. Past* **10**, 591–605 (2014).
32. J. D. Shakun, P. U. Clark, F. He, S. A. Marcott, A. C. Mix, Z. Liu, B. Otto-Bliesner, A. Schmittner, E. Bard, Global warming preceded by increasing carbon dioxide concentrations during the last deglaciation. *Nature* **484**, 49–54 (2012).
33. J. F. McManus, R. Francois, J.-M. Gherardi, L. D. Keigwin, S. Brown-Leger, Collapse and rapid resumption of Atlantic meridional circulation linked to deglacial climate changes. *Nature* **428**, 834–837 (2004).
34. C. Buizert, M. Sigl, M. Severi, B. R. Markle, J. J. Wettstein, J. R. McConnell, J. B. Pedro, H. Sodemann, K. Goto-Azuma, K. Kawamura, S. Fujita, H. Motoyama, M. Hirabayashi, R. Uemura, B. Stenni, F. Parrenin, F. He, T. J. Fudge, E. J. Steig, Abrupt ice-age shifts in southern westerly winds and Antarctic climate forced from the north. *Nature* **563**, 681–685 (2018).
35. WAIS Divide Project Members, Precise interpolar phasing of abrupt climate change during the last ice age. *Nature* **520**, 661–665 (2015).
36. J. M. Lauderdale, R. G. Williams, D. R. Munday, D. P. Marshall, The impact of Southern Ocean residual upwelling on atmospheric CO_2 on centennial and millennial timescales. *Clim. Dynam.* **48**, 1611–1631 (2017).
37. C. Völker, P. Köhler, Responses of ocean circulation and carbon cycle to changes in the position of the Southern Hemisphere westerlies at Last Glacial Maximum. *Paleoceanography* **28**, 726–739 (2013).
38. J. B. Pedro, M. Jochum, C. Buizert, F. He, S. Barker, S. O. Rasmussen, Beyond the bipolar seesaw: Toward a process understanding of interhemispheric coupling. *Quat. Sci. Rev.* **192**, 27–46 (2018).
39. J.-M. Gherardi, L. Labeyrie, S. Nave, R. Francois, J. F. McManus, E. Cortijo, Glacial-interglacial circulation changes inferred from $^{231}Pa/^{230}Th$ sedimentary record in the North Atlantic region. *Paleoceanography* **24**, PA2204 (2009).
40. J. W. B. Rae, W. Broecker, What fraction of the Pacific and Indian oceans' deep water is formed in the Southern Ocean? *Biogeosciences* **15**, 3779–3794 (2018).
41. S. Barker, P. Diz, M. J. Vautravers, J. Pike, G. Knorr, I. R. Hall, W. S. Broecker, Interhemispheric Atlantic seesaw response during the last deglaciation. *Nature* **457**, 1097–1102 (2009).
42. T. K. Bauska, D. Baggenstos, E. J. Brook, A. C. Mix, S. A. Marcott, V. V. Petrenko, H. Schaefer, J. P. Severinghaus, J. E. Lee, Carbon isotopes characterize rapid changes in atmospheric carbon dioxide during the last deglaciation. *Proc. Natl. Acad. Sci. U.S.A.* **113**, 3465–3470 (2016).
43. A. L. Gordon, B. A. Huber, Southern Ocean winter mixed layer. *J. Geophys. Res. Oceans* **95**, 11655–11672 (1990).
44. J. B. Pedro, T. Martin, E. J. Steig, M. Jochum, W. Park, S. O. Rasmussen, Southern Ocean deep convection as a driver of Antarctic warming events. *Geophys. Res. Lett.* **43**, 2192–2199 (2016).
45. A. Schmittner, E. J. Brook, J. Ahn, Impact of the ocean's overturning circulation on atmospheric CO_2, in *Ocean Circulation: Mechanisms and Impacts-Past and Future Changes of Meridional Overturning* (2007), pp. 315–334.
46. J. Toggweiler, D. W. Lea, Temperature differences between the hemispheres and ice age climate variability. *Paleoceanography* **25**, PA2212 (2010).
47. J. Yu, W. S. Broecker, H. Elderfield, Z. Jin, J. McManus, F. Zhang, Loss of carbon from the deep sea since the last Glacial Maximum. *Science* **330**, 1084–1087 (2010).
48. W. S. Broecker, T.-H. Peng, The role of $CaCO_3$ compensation in the glacial to interglacial atmospheric CO_2 change. *Global Biogeochem. Cycles* **1**, 15–29 (1987).
49. H. Huang, M. Gutjahr, A. Eisenhauer, G. Kuhn, No detectable weddell sea antarctic bottom water export during the last and penultimate Glacial Maximum. *Nat. Commun.* **11**, 424 (2020).
50. P. T. Spooner, T. Chen, L. F. Robinson, C. D. Coath, Rapid uranium-series age screening of carbonates by laser ablation mass spectrometry. *Quat. Geochronol.* **31**, 28–39 (2015).
51. A. Burke, L. F. Robinson, A. P. McNichol, W. J. Jenkins, K. M. Scanlon, D. S. Gerlach, Reconnaissance dating: A new radiocarbon method applied to assessing the temporal distribution of Southern Ocean deep-sea corals. *Deep Sea Res. I Oceanogr. Res. Pap.* **57**, 1510–1520 (2010).
52. A. R. Margolin, L. F. Robinson, A. Burke, R. G. Waller, K. M. Scanlon, M. L. Roberts, M. E. Auro, T. van de Flierdt, Temporal and spatial distributions of cold-water corals in the Drake Passage: Insights from the last 35,000 years. *Deep Sea Res. II Top. Stud. Oceanogr.* **99**, 237–248 (2014).
53. L. I. Bradtmiller, L. F. Robinson, J. F. McManus, M. E. Auro, H. C. Bostock, The distribution of ^{231}Pa and ^{230}Th in paired water column and surface sediment samples. *Geochim. Cosmochim. Acta* **73**, A154 (2009).
54. R. L. Edwards, C. D. Gallup, H. Cheng, Uranium-series dating of marine and lacustrine carbonates. *Rev. Mineral. Geochem.* **52**, 363–405 (2003).
55. T. Chen, L. F. Robinson, M. P. Beasley, L. M. Claxton, M. B. Andersen, L. J. Gregoire, J. Wadham, D. J. Fornari, K. S. Harpp, Ocean mixing and ice-sheet control of seawater $^{234}U/^{238}U$ during the last deglaciation. *Science* **354**, 626–629 (2016).
56. L. F. Robinson, G. M. Henderson, L. Hall, I. Matthews, Climatic control of riverine and seawater uranium-isotope ratios. *Science* **305**, 851–854 (2004).
57. P. J. Reimer, M. G. L. Baillie, E. Bard, A. Bayliss, J. W. Beck, P. G. Blackwell, C. Bronk Ramsey, C. E. Buck, G. S. Burr, R. L. Edwards, M. Friedrich, P. M. Grootes, T. P. Guilderson, I. Hajdas, T. J. Heaton, A. G. Hogg, K. A. Hughen, K. F. Kaiser, B. Kromer, F. G. McCormac, S. W. Manning, R. W. Reimer, D. A. Richards, J. R. Southon, S. Talamo, C. S. M. Turney, J. van der Plicht, C. E. Weyhenmeyer, IntCal09 and Marine09 radiocarbon age calibration curves, 0–50,000 years cal BP. *Radiocarbon* **51**, 1111–1150 (2009).
58. J. S. Vogel, J. R. Southon, D. Nelson, T. A. Brown, Performance of catalytically condensed carbon for use in accelerator mass spectrometry. *Nucl. Instrum. Methods Phys. Res. Sect. B* **5**, 289–293 (1984).
59. I. U. Olsson, *Radiocarbon Variations and Absolute Chronology* (Wiley Interscience Division, 1970).
60. M. Stuiver, H. A. Polach, Discussion reporting of ^{14}C data. *Radiocarbon* **19**, 355–363 (1977).
61. M. S. Cook, L. D. Keigwin, Radiocarbon profiles of the NW Pacific from the LGM and deglaciation: Evaluating ventilation metrics and the effect of uncertain surface reservoir ages. *Paleoceanography* **30**, 174–195 (2015).
62. A. Verdy, M. R. Mazloff, A data assimilating model for estimating Southern Ocean biogeochemistry. *J. Geophys. Res. Oceans* **122**, 6968–6988 (2017).
63. A. Olsen, R. M. Key, S. van Heuven, S. K. Lauvset, A. Velo, X. Lin, C. Schirnick, A. Kozyr, T. Tanhua, M. Hoppema, S. Jutterström, R. Steinfeldt, E. Jeansson, M. Ishii, F. F. Pérez, T. Suzuki, The Global Ocean Data Analysis Project version 2 (GLODAPv2)—An internally consistent data product for the world ocean. *Earth Syst. Sci. Data* **8**, 297–323 (2016).
64. R. Schlitzer, *Ocean Data View* (2016); http://odv.awi.de
65. EPICA Community Members, One-to-one coupling of glacial climate variability in Greenland and Antarctica. *Nature* **444**, 195–198 (2006).
66. C. Buizert, V. Gkinis, J. P. Severinghaus, F. He, B. S. Lecavalier, P. Kindler, M. Leuenberger, A. E. Carlson, B. Vinther, V. Masson-Delmotte, J. W. C. White, Z. Liu, B. Otto-Bliesner, E. J. Brook, Greenland temperature response to climate forcing during the last deglaciation. *Science* **345**, 1177–1180 (2014).
67. D. Veres, L. Bazin, A. Landais, H. Toyé Mahamadou Kele, B. Lemieux-Dudon, F. Parrenin, P. Martinerie, E. Blayo, T. Blunier, E. Capron, J. Chappellaz, S. O. Rasmussen, M. Severi, A. Svensson, B. Vinther, E. W. Wolff, The Antarctic ice core chronology (AICC2012): An optimized multi-parameter and multi-site dating approach for the last 120 thousand years. *Clim. Past* **9**, 1733–1748 (2013).
68. M. P. Hain, D. M. Sigman, G. H. Haug, Distinct roles of the Southern Ocean and North Atlantic in the deglacial atmospheric radiocarbon decline. *Earth Planet. Sci. Lett.* **394**, 198–208 (2014).
69. G. A. Kovaltsov, A. Mishev, I. G. Usoskin, A new model of cosmogenic production of radiocarbon ^{14}C in the atmosphere. *Earth Planet. Sci. Lett.* **337**, 114–120 (2012).

70. J. P. Sachs, R. F. Anderson, Fidelity of alkenone paleotemperatures in southern Cape Basin sediment drifts. *Paleoceanography* **18**, 1082 (2003).
71. F. Lambert, M. Bigler, J. P. Steffensen, M. Hutterli, H. Fischer, Centennial mineral dust variability in high-resolution ice core data from Dome C, Antarctica. *Clim. Past* **8**, 609–623 (2012).

Acknowledgments: We thank D. Sigman for comments during the preparation of this manuscript and C. Coath and C. Taylor for help in the laboratory. Reviews by the editor D. Lea and four anonymous reviewers improved the manuscript. **Funding:** Support for this work comes from the European Research Council, the Natural Environmental Research Council, the U.S. NSF, the National Oceanic and Atmospheric Administration (NOAA) Ocean Exploration Trust, the Royal Society Newton Mobility Grant in conjunction with the National Natural Science Foundation of China (no. 41711530222), the National Natural Science Foundation of China (nos. 41991325, 41822603, and 91955201), the China Scholarship Council, and the program A for outstanding Ph.D. candidate of Nanjing University. Computational resources for the SOSE are provided by NSF XSEDE resource grant OCE130007. **Author contributions:** T.L., L.F.R., and T.C. designed the study. T.L., L.F.R., T.C., A.B., A.P-H., A.S., G.H.R., J.A.S., and P.T.S. collected and U-Th–dated the deep-sea coral samples. T.L., T.C., A.P-H., T.D.J.K., and J.S. made the radiocarbon analyses. T.L., L.F.R., T.C., J.W.B.R., and A.B. made the interpretations and wrote the first draft. All authors contributed to refinements of the interpretations and editing of the manuscript. **Competing interests:** The authors declare that they have no competing interests. **Data and materials availability:** All data needed to evaluate the conclusions in the paper are present in the paper and/or the Supplementary Materials. Additional data related to this paper may be requested from the authors.

Submitted 19 February 2020
Accepted 25 August 2020
Published 16 October 2020
10.1126/sciadv.abb3807

Citation: T. Li, L. F. Robinson, T. Chen, X. T. Wang, A. Burke, J. W. B. Rae, A. Pegrum-Haram, T. D. J. Knowles, G. Li, J. Chen, H. C. Ng, M. Prokopenko, G. H. Rowland, A. Samperiz, J. A. Stewart, J. Southon, P. T. Spooner, Rapid shifts in circulation and biogeochemistry of the Southern Ocean during deglacial carbon cycle events. *Sci. Adv.* **6**, eabb3807 (2020).

ScienceAdvances

Rapid shifts in circulation and biogeochemistry of the Southern Ocean during deglacial carbon cycle events

Tao LiLaura F. RobinsonTianyu ChenXingchen T. WangAndrea BurkeJames W. B. RaeAlbertine Pegrum-HaramTimothy D. J. KnowlesGaojun LiJun ChenHong Chin NgMaria ProkopenkoGeorge H. RowlandAna SamperizJoseph A. StewartJohn SouthonPeter T. Spooner

Sci. Adv., 6 (42), eabb3807. • DOI: 10.1126/sciadv.abb3807